1 # Wind and Phytoplankton Dynamics Drive Seasonal and Short-Term
2 # Variability of Suspended Matter in a Tidal Basin

3 **Gaziza Konyssova[1,2*], Vera Sidorenko[1,2], Alexey Androsov[1,2], Sabine Horn[2], Sara Rubinetti[1,3],**
4 **Ivan Kuznetsov[1], Karen Helen Wiltshire[2,4], Justus van Beusekom[2,5]**

5 [1] Alfred-Wegener-Institut Helmholtz-Zentrum für Polar- und Meeresforschung, Bremerhaven, Germany
6 [2] Wadden Sea Station Sylt, Alfred-Wegener-Institut Helmholtz-Zentrum für Polar- und
7 Meeresforschung, List/Sylt, Germany
8 [3] Dipartimento per lo Sviluppo Sostenibile e la Transizione Ecologica, University of Piemonte
9 Orientale, Vercelli, Italy
10 [4] Climate Science Trinity College Dublin, Dublin, Ireland
11 [5] Institute for Carbon Cycles, Helmholtz Centre Hereon, Geesthacht, Germany

12 *** Correspondence:**
13 Gaziza Konyssova
14 gaziza.konyssova@awi.de
15 ORCID: 0009-0008-5460-4754

16 **Abstract**
17 Suspended particulate matter (SPM) is a key component of coastal ecosystems, modulating light
18 availability, nutrient transport, and food web dynamics. Its variability is driven by a combination of
19 physical and biological processes that interact across temporal and spatial scales. Using the Sylt-Rømø
20 Bight as a natural laboratory and focusing on the period 2000-2019, in this study, we integrate statistical
21 analysis of observational data from the Sylt Roads monitoring program and local meteorological
22 stations, neural network modelling and Lagrangian transport simulations. This multi-method approach
23 enables us to disentangle and quantify the relative roles of tidal and wind forcing, as well as biological
24 processes in shaping SPM concentrations across various time scales, based on near-surface
25 measurements at two monitoring stations.
26 The findings show that wind intensity dominates short-term SPM variability, particularly at the shallow
27 station, where SPM responds rapidly to local wind-induced resuspension. At the deep station, the wind
28 effects appear with a delay of ~5 days, aligning with tidally induced transport timescales (~133 hours)
29 from shallower resuspension zones, as revealed by Lagrangian simulations. Seasonal patterns are
30 further modulated by both reduced wind intensities and the onset of biological processes, such as
31 phytoplankton blooms, which promote flocculation and subsequent settling in spring and summer.
32 Neural network experiments highlight the shifting seasonal balance between physical and biological
33 controls. The median concentration of SPM decreased by up to 80% from winter to summer.
34 Approximately 40% of this seasonal difference can be attributed to weaker wind conditions, while the
35 remaining ~40% is likely driven by biologically mediated sinking processes.

1 Introduction

Suspended particulate matter (SPM) is a key component of coastal systems, influencing a wide range of physical and ecological processes. It consists of a mixture of small solid particles of both organic and inorganic origin suspended in the water column with concentrations, size (Eisma, 1986) and composition varying spatially and temporally (Schartau et al., 2019). The spatiotemporal variation in SPM concentrations is driven by an interplay of hydrodynamic, meteorological, and biological factors, which in turn, regulate nutrient availability, light penetration, and organic matter distribution. This directly impacts ecosystem productivity, including the timing of the phytoplankton bloom in spring (Cadée, 1986) and spatial gradients in primary productivity (Cloern, 1987; Colijn, 1982), and trophic interactions (Dolch and Reise, 2010; Graf and Rosenberg, 1997).

In tidally energetic environments like the Wadden Sea, the suspended matter gradient is kept upright by the density-driven coastward transport of bottom water and tidal straining (Becherer et al., 2016; Burchard et al., 2008; Flöser et al., 2011). Sediment accumulation is further influenced by hydrodynamic retention mechanisms such as enhanced settling due to the landward dissipation of current velocity, the scour-lag (Dyer, 1995; Friedrichs and Aubrey, 1988) and settling lag effects (Postma, 1967), and the tidal asymmetry formed by the presence of non-linear processes within the tidal system (Dronkers, 1986; Fofonova et al., 2019; Friedrichs and Aubrey, 1988; Hagen et al., 2022). The role of tidal currents in the variability of SPM concentrations is found to be significant through transport processes (Bartholomä et al., 2009; Christiansen et al., 2006) as well as sediment erosion even under calm and moderate weather conditions (Bartholomä et al., 2009; Lettmann et al., 2009). While tides regulate advection and maintain a baseline shear stress, the co-occurrence of strong winds and wave-induced turbulence during severe weather further enhances bottom stress and promotes additional erosion.

Wind stress and wave action are critical in short-term SPM dynamics. Wind-induced resuspension, particularly in shallow coastal areas, causes episodic increases in turbidity (Aarup, 2002; Fettweis et al., 2012). Stronger and more persistent wind forcing during winter maintains higher SPM concentrations, keeping fine sediments in suspension (de Jonge and van Beusekom, 1995; van Beusekom et al., 1999), while calmer conditions in summer enable enhanced settling (Bale et al., 1985; Verney et al., 2009). Beyond physical resuspension and transport mechanisms, biochemical processes also influence SPM concentrations by modulating aggregation, stabilization, and vertical flux of particulate matter (de Jonge and van Beusekom, 1995; van Beusekom and de Jonge, 2002; Verney et al., 2009). For example, flocculation, the aggregation and breakup of particles, is a key mechanism by which biological activity modulates SPM concentrations (Wotton, 2004; Eisma, 1986). Phytoplankton blooms in spring and summer can promote flocculation, leading to enhanced particle settling and reduced SPM concentrations in the water column (de Jonge & van Beusekom, 1995; Schartau et al., 2019). The process is particularly enhanced by the occurrence of extracellular polymeric substances (EPS), including marine gels such as transparent exopolymeric particles (TEPs), but can also occur due to cohesive properties of fine-grained minerals like clays (Passow, 2002; Verney et al., 2009). The size and cohesiveness of these biologically mediated flocs also govern their settling velocities and resuspension thresholds, affecting how quickly particles are redistributed in the water column. Warmer temperatures also accelerate the decomposition of organic matter (OM), which is nearly always present

78 in natural flocs in various forms (detritus, adsorbed OM molecules, and living OM), and may range
79 from a minor to a dominant fraction of total floc mass (Eisma, 1986; Engel and Schartau, 1999). This
80 directly links SPM dynamics to food-web functioning (Wotton, 2004; Engel & Schartau, 1999). In
81 addition, temperature also affects top-down controls such as zooplankton grazing, which alters SPM
82 composition and concentration through multiple pathways. Grazing modifies the SPM field not only
83 through phytoplankton consumption but also via the fragmentation of aggregates, production of fecal
84 pellets and organic material that promote microbial and TEP-mediated aggregation. The effects of these
85 processes can either promote particle settling or enhance recycling and suspension, depending on
86 community composition, feeding modes, and environmental conditions (e.g., Passow, 2002; Toullec et
87 al., 2019; Turner, 2002).
88 In the shallow coastal systems, light can reach the seafloor, stimulating benthic algae growth, provided
89 water clarity allows sufficient light penetration (Loebl et al., 2007). These benthic processes further
90 influence SPM concentrations through both stabilization and removal mechanisms. While
91 microphytobenthos, consisting of benthic diatoms and cyanobacteria, produce biofilms that stabilize
92 sediments and reduce resuspension (Stal, 2010), filter-feeding organisms, such as mussels (*Mytilus*
93 *edulis*) and oysters (*Magallana gigas*), alter SPM dynamics by removing fine particles from suspension,
94 affecting both sediment deposition rates and nutrient cycling (Graf and Rosenberg, 1997). Moreover,
95 excessive nutrient loads can enhance phytoplankton blooms, whose decay products and extracellular
96 polymeric substances facilitate biomineral floc formation (Passow, 2002; van Beusekom et al., 1999),
97 which promotes OM sedimentation and alters benthic-pelagic coupling by influencing the availability of
98 organic matter to both suspension and deposit feeders. These processes collectively shape coastal
99 sediment dynamics, contributing to the long-term evolution of tidal flat environments.
100 While hydrodynamic and wind-driven influences on SPM have been extensively studied, their
101 interaction with biological processes and relative contributions remain incompletely understood, despite
102 growing interest. By leveraging long-term ecological monitoring data from the Sylt Roads program, this
103 study aims to quantify the contributions of tidally induced and wind-driven resuspension and transport,
104 as well as biologically mediated processes, to the spatiotemporal variability of SPM in the Sylt-Rømø
105 Bight.
106 This analysis integrates high-resolution in situ measurements from two Long-Term Ecological Research
107 (LTER) stations from 2000 to 2019, meteorological data from the station List (Sylt, Germany), and
108 outputs from hydrodynamic and neural network modelling to evaluate SPM dynamics across short-term
109 (hourly to daily) and seasonal timescales. The following research questions guide the study: (1) What
110 are the dominant mechanisms driving SPM variability across different temporal scales? (2) How do
111 these mechanisms differ between the two monitoring stations within the Sylt-Rømø Bight? (3) How
112 important are biological processes in shaping observed SPM concentrations?

2 Data and Methods

2.1 Area Description

The investigations were carried out in the Sylt-Rømø Bight, a shallow, tidal basin in the northern Wadden Sea (southeastern North Sea; see Fig. 1). The basin is semi-enclosed due to two causeways at its northern and southern ends, isolating it from neighboring basins. Its only connection to the North Sea is through the deep tidal inlet Lister Deep, between the islands of Sylt and Rømø. The bay spans approximately 410 km² and features a highly variable topography, including extensive intertidal flats (>45%), shallow subtidal zones (~35%), and deep tidal channels (~10%). The Sylt-Rømø Bight's bathymetry is characterised by a mean water depth of approximately 4 m, with a maximum depth of about 37 m observed in the tidal inlet Lister Deep. Most subtidal and ~72% of intertidal sediments are sand-dominated. The basin also features a small sheltered embayment Königshafen, with an average depth of ~2m and encompasses large areas which become exposed at low tides.
The tidal range in the bight averages 2 m, based on observations at the List tide gauge (E.U. Copernicus Marine Service Information, doi.org/10.48670/moi-00036). Tidal forcing accounts for over 80% of depth-averaged velocity variability under regular wind conditions, in the absence of storms, and over 90% during spring tides (Fofonova et al., 2019). The bight receives minimal fluvial input, with small rivers such as the Vidå and Brede Å (see Fig.1), contributing only 4–10 m³/s of freshwater (Purkiani et al., 2015). Water exchange with the open North Sea occurs exclusively through Lister Deep, a 2.8 km wide tidal inlet. At the mouth of Lister Deep, a prominent ebb-tidal delta extends seaward, acting as both a sediment trap and a pathway for sediment redistribution within the bight (Dissanayake et al., 2012). Localized anthropogenic disturbance may also influence sediment availability and distribution in the region, although detailed records of maritime traffic, dredging operations, and benthic trawling specific to the Sylt-Rømø Bight are limited. However, studies from the broader Wadden Sea show that anthropogenic activities such as bottom trawling (e.g., Bruns et al., 2023; Depestele et al., 2016), dredging (de Jonge and de Jong, 2002; de Jonge, 1983; van Maren et al., 2015), and mussel farming (Jansen et al., 2023) are recognized drivers of sediment disturbance and resuspension.

143
144 **Figure 1: Map of the Sylt-Rømø Bight showing bathymetry, key habitats (tidal flats, bivalve beds, seagrass meadows, and salt**
145 **marshes), LTER sampling stations (Deep Station – Lister Ley; Shallow Station – Königshafen), tide gauge locations (List,**
146 **Havneby, Vidå), and rivers (Brede Å and Vidå). The basin is connected to the North Sea via the tidal inlet Lister Deep and**
147 **laterally enclosed by causeways to the north and south.**

148 **2.2 FESOM-C Model**

149 This study used the coastal hydrodynamic model FESOM-C (Androsov et al., 2019). FESOM-C is
150 designed explicitly for high-resolution coastal applications and employs a finite-volume cell-vertex

151 discretization on unstructured meshes composed of triangles and quadrilaterals. This allows for flexible
152 spatial resolution down to several metres, suitable for simulating complex coastal dynamics (Fofonova
153 et al., 2019; Kuznetsov et al., 2020, 2024; Neder et al., 2022; Sprong et al., 2020; Sidorenko et al.,
154 2025).

2.2.1 Model Setup

156 The setup utilized an unstructured hybrid mesh of 208,345 nodes and 211,545 elements. Due to the
157 semi-enclosed state of the bight, the mesh contains a single open boundary at the seaward edge of the
158 domain, connecting the basin with the North Sea. The horizontal spatial resolution varies from up to 2
159 m in wetting-drying zones to 304 m in the deeper outer part (near the open boundary). The experiments
160 were carried out by running 2D barotropic simulations with the wetting/drying option enabled to
161 capture the periodic submergence and exposure of intertidal areas. The model timestep was set to ~ 0.25
162 seconds, with data output every ~20 minutes of simulation time. The bottom friction coefficient was
163 applied as 0.0025, a value identified as optimal in prior studies of the same study area when using
164 TPXO9 tidal solution (Fofonova et al., 2019; Konyssova et al., 2025).
165 The simulations are driven by tidal forcing alone, applied at the open boundary. For an accurate
166 simulation of the tidal dynamics, thirteen major tidal harmonic constituents (M2, S2, N2, K2, K1, O1,
167 P1, Q1, Mm, Mf, MN4, 2N, and S1) and two over-harmonics (M4, MS4) were prescribed by their
168 phases and amplitudes at the open boundary based on TPXO9 tidal atlas (Egbert and Erofeeva, 2002).
169 This selection of the tidal solution was justified by its robust performance and is one of the most
170 optimal for the North Sea (Fofonova et al., 2019). The current setup has been validated in a previous
171 work by Konyssova et al. (2025). The model's performance has been validated using tidal gauge (TG)
172 data from stations List, Vidå, and Havneby (see Fig. 1; performance results are provided in the
173 Supplementary Materials, Table S1). Since the numerical setup remains unchanged, we refer to
174 Konyssova et al. (2025) for full validation details.

2.2.2 Lagrangian Module

176 To assess tidally driven spatial connectivity and transport timescales within the basin, we performed
177 Lagrangian simulations using FESOM-C Drift, a post-processing tool designed for particle tracking.
178 The model advects massless passive particles based on the velocity fields produced by the
179 hydrodynamic model. In this study, we use the term "passive tracers" to denote Lagrangian particles
180 without weight or settling properties. This is equivalent to virtual Lagrangian particles commonly
181 applied in particle tracking studies and should not be confused with dye experiments that represent
182 concentration changes in space and time.
183 The experiment involved releasing passive tracers from all grid elements within the domain that are
184 consistently inundated during every flood phase. We released about 90,000 tracers at three-hour
185 intervals over six weeks (169 iterations in total). Each tracer was tracked for up to three weeks and was
186 removed from the simulation once it reached either of the two Sylt Roads sampling stations (see Fig. 1
187 and Section 2.3.1). The iterative release process was designed to capture the full range of tidal
188 conditions and the complexity of hydrodynamic transport within the basin, ensuring that the results are

190 statistically robust. Upon arrival at a station, tracers were immediately removed to prevent post-arrival
191 movements from influencing the mapped source regions and transport pathways. The simulations were
192 conducted independently for each station, focusing exclusively on the paths from the release locations
193 to the respective sampling site. If a tracer did not reach the designated station within the simulation time
194 frame, it was considered to originate from a region that falls outside the station's dominant transport
195 pathways.
196 The first analysis approach assessed the source regions of passive tracers arriving at the sampling
197 stations. This allows us to evaluate the connectivity between different subareas of the basin and the
198 sampling sites. The probability of SPM originating from a given area was mapped based on the
199 cumulative occurrence of tracer pathways across all iterations. Higher probability values indicate areas
200 that more frequently serve as source regions or transport pathways for SPM reaching the sampling
201 stations.
202 The second part of the analysis was conducted to estimate the mean transit time of the tracers reaching
203 the sampling stations from shallow source zones, where resuspension typically occurs (defined here as
204 areas <2 m deep, based on de Jonge & van Beusekom, 1995). The mean transit time over all
205 implementations was calculated for all elements whose tracers reached the stations within the simulated
206 three weeks. To quantify how long it typically takes for high tracer concentrations to reach the station,
207 we computed a probability-weighted median transit time, where mean transit times were weighted by
208 their probability values. This approach ensures that frequent transport pathways are given greater
209 influence in the median transit time calculation, reducing bias from rare, low-probability trajectories.

210 **2.3 Data**

211 **2.3.1 Biogeochemistry data**

212 This study used data from the Sylt Roads long-term ecological monitoring program, focusing on a
213 subset from 2000 to 2019 to ensure consistent methodology and regular sampling. From a broad range
214 of hydrographic and biogeochemical parameters covered in the dataset, this study specifically analyzed
215 suspended particulate matter (SPM; mg/L, filtered through 0.4 μm nucleopore filters, rinsed with
216 distilled water, stored frozen, and dried at 60 °C) and chlorophyll-a (Chl-a; μg/L, filtered through GF/C
217 filters (Whatman), stored at −20 °C, and extracted using 90% acetone and analyzed
218 spectrophotometrically using the trichromatic method as described by Jeffrey and Humphrey, (1975).
219 Both parameters were measured twice weekly at a sampling depth of 1 m below the surface at two
220 primary stations: the deep station at the Lister Ley channel and the shallow station at the entrance of
221 Königshafen embayment (see Fig. 1). The full dataset is publicly available on the data portal
222 PANGAEA (https://www.pangaea.de) and the recent evaluation is detailed in Rick et al. (2023).
223 To analyze seasonal variability, we defined the seasons based on observed cycles in Chl-a
224 concentrations at the study site, rather than calendar or astronomical definitions. Specifically, we used:
225 - winter (November 20 – February 19, low biological activity, low Chl-a);
226 - spring (February 20 – May 31, phytoplankton bloom initiation and peak);
227 - summer (June 1 – September 19, post-bloom conditions, high light, reduced Chl-a);
228 - autumn (September 20 – November 20, transitional period).

2.3.2 Meteorological data

229

230 For the statistical analysis, we also downloaded the quality checked historical meteorological data for
231 station 3032, List auf Sylt, from Climate Data Center (CDC) of the Deutscher Wetterdienst (DWD).
232 The data includes hourly mean wind speed and wind direction (dataset ID: urn:x-
233 wmo:md:de.dwd.cdc::obsgermany-climate-hourly-wind), and daily sunshine duration (dataset ID:
234 urn:wmo:md:de-dwd-cdc:obsgermany-climate-daily-kl).

2.3.3 Sea Surface Height data

235

236 Using the validated model setup (Fofonova et al., 2019; Konyssova et al., 2025), the sea surface height
237 (SSH) data were reconstructed for the deep and shallow stations. In particular, the amplitudes and
238 phases of the 15 harmonics mentioned above were obtained from the modeling output using Fast
239 Fourier Transform analysis. Subsequently, the SSH signal was reconstructed for the exact timestamps
240 of the LTER sampling using the *t_tide* package (Pawlowicz et al., 2002). This allowed us to estimate
241 the tidal elevation and phase (through the SSH and SSH gradients) at the time of sampling, which were
242 then included as input features in the statistical and neural network (NN) analyses. Their relationship is
243 illustrated and discussed in Supplementary Material, Figs. S3–S4.

244 **Table 1. The physical and hydrochemical parameters used in the study (short name, units, frequency, and source)**

Data	Unit	Frequency	Source
SPM	mg/L	twice weekly	Sylt Roads Marine Observatory
Chl-a	µg/L	twice weekly	Sylt Roads Marine Observatory
Wind speed and direction	m/s, degrees	hourly mean	Deutscher Wetterdienst
Light	hours	daily	Deutscher Wetterdienst
SSH	m	every 5 minutes	Model reconstruction using 13 harmonics and 2 over-harmonics from TPXO9 and verified with the tidal gauges

2.4 Neural Network

245

246 To assess the relative contribution of biotic conditions to SPM concentrations, we employed a forward
247 NN to predict SPM based on environmental input parameters. The approach relies primarily on long-
248 term observational data, thereby enhancing the robustness of the results, complemented by model-
249 derived SSH and its temporal gradient data. Although numerical simulations are also powerful tools in
250 this context, any discrepancies they produce can largely be attributed to the choice of numerical
251 methods and the associated uncertainties, including unresolved processes, boundary conditions, and the
252 spatial and temporal resolution of both modelled and observed data (Skogen et al, 2021). While it does
253 not provide process-based understanding, the NN approach is particularly well-suited for this task, as it
254 offers a cost-efficient and data-driven means to capture complex, non-linear relationships between
255 influencing factors. We conducted several sensitivity experiments (not shown), varying both the

261 network depth and the number of neurons per layer. For the current application, increasing the network
262 depth further did not improve performance.
263 For the first part of the experiment, the primary regression task involved predicting SPM concentrations
264 during the winter season, which is characterized by low biological activity, as indicated by minimal
265 Chl-a concentrations. Focusing on winter allows for a clearer assessment of physical (abiotic) drivers,
266 such as wind forcing, with reduced biological confounding. The input features, 19 in total, of the NN
267 model include wind magnitude at the time of sampling and averages over a series of prior time intervals
268 (6 to 240 hours, corresponding to the intervals analyzed in Subsection 3.2.2), dominant wind direction
269 over 6 and 12 hours (even though the correlation analysis shows only a minor impact, the non-linear
270 effects of wind direction may still be present), salinity, SSH, and the temporal gradient of SSH
271 (computed using a forward scheme). The results of the winter model are presented in Section 3.3.1.
272 To extend the analysis across seasons, we applied the same model architecture to the full dataset,
273 initially using the same input features as in the winter setup (results in Section 3.3.3), and subsequently
274 incorporating two additional features: temperature and the weekly sum of sunshine hours before the
275 measurement date (21 features in total, Section 3.3.4). The latter serve as a pragmatic proxy for both
276 Chl-a concentration and benthic algae abundance. While we do not attempt to separate these
277 mechanisms individually, this approach is exploratory and intended to approximate their combined
278 influence on seasonal SPM variability.
279 The technical details of the NN architecture are provided in the Supplementary Material, together with
280 the complete predictor list in Table S2.

281 **3 Results**

282 Figure 2 presents the time series of SPM concentrations at the deep and shallow stations in the Sylt-
283 Rømø Bight from 2000 to 2019, based on data from the Sylt Roads monitoring program (Section 2.3.1;
284 station locations shown in Fig. 1). Both stations display a pronounced seasonal cycle, with SPM
285 concentrations typically peaking in winter and declining during summer. The deep station shows more
286 frequent and sustained seasonal peaks in SPM concentrations throughout the time series, whereas the
287 shallow station tends to exhibit higher concentrations during peak events. It is also important to note
288 that the regular sampling at the shallow station was discontinued after 2013 following the replacement
289 of the research vessel, resulting in reduced data coverage in subsequent years.

Figure 2: Time series of SPM for the considered years (2000–2019) for the deep (blue) and shallow stations (orange) gridded per year. Each subplot represents a calendar year with time on the x-axis and SPM concentration [mg/l] on the y-axis.

3.1 Seasonality of SPM concentrations

SPM concentrations show an apparent seasonality, which is further investigated in relation to biological activity and meteorological drivers in the subsequent analyses. Using Chl-a as a proxy for phytoplankton biomass, this subsection applies statistical analysis to examine how biological activity and wind forcing together shape seasonal patterns of SPM variability at both the deep and shallow stations.

3.1.1 Role of biological processes in seasonal SPM variations

Both stations exhibit distinct seasonal variations in SPM and Chl-a concentrations (Fig. 3). SPM concentrations are highest in late autumn and winter, with median values of about ~28 mg/L (33.9 ± 18.2 mg/L) at the deep and median of ~26 mg/L (38.6 ± 16.4 mg/L) at the shallow stations. In January, the peak reaches over 60 mg/L at both stations, with individual events exceeding 70 mg/L. The decline in concentrations is observed from February to May, reaching their lowest values in June to August (around 2-3 mg/L), although occasional peaks above 30-40 mg/L still occur. From September onward, SPM begins to increase. This pattern is similar at both stations, though the shallow station generally has slightly higher SPM concentrations, suggesting potential differences in sediment availability or resuspension dynamics.

Chlorophyll-a concentrations follow an inverse seasonal pattern. It remains low in December–January with a median around 2 µg/L (2.1 ± 0.7 µg/L) at both stations. It increases sharply in early spring, with peaks in March-April exceeding 30 µg/L at the deep station and 25 µg/L at the shallow station. Concentrations then drop in summer, followed by a secondary increase in August–October, when values up to ~15-20 µg/L are observed.
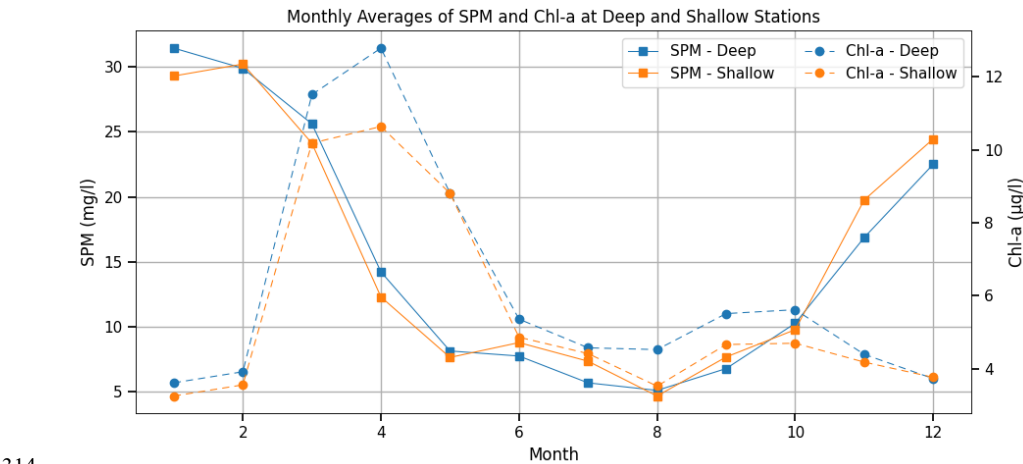
Figure 3: Monthly averages of SPM and Chl-a at the deep (blue) and shallow (orange) stations for the considered years (2000– 2019). SPM concentrations solid line with square marker, left axis) and Chl-a concentrations (dashed line with circle markers, right axis) are displayed separately for clarity. The x-axis represents the months from January to December.

The relationship between Chl-a and SPM varies across seasons (Fig. 4). During December–February, biological activity is low and Chl-a constitutes a relatively constant fraction of total SPM, both subject to the same resuspension-deposition processes. This co-settling behavior leads to strong positive correlations observed at both stations. The highest values occur at the shallow station, with $R^2 = 0.84$ in December and $R^2 = 0.75$ in January. At the deep station, correlations are relatively lower, reaching $R^2 =$

323   0.52 in December and $R^2 = 0.56$ in January. The strong correlation and the slope are in line with the
324   resuspension of microphytobenthos as observed in winter by de Jonge and van Beusekom (1995). From
325   March onward, the relationship becomes more complex. As Chl-a rises rapidly during the spring bloom
326   and SPM concentrations decline, the correlation at both stations weakens with R^2 values dropping to
327   near-zero in March. This divergence reflects differences in vertical distribution and settling behavior.
328   While phytoplankton is a component of SPM and both are retained on the filter, their decoupling in
329   spring and summer may reflect that not all phytoplankton is floc-associated. Active phytoplankton may
330   remain suspended near the surface, while denser biomineral flocs sink more rapidly, leading to weaker
331   correlations in integrated surface samples. This non-linear and temporally variable influence of Chl-a
332   also underlies the decision not to use it directly as a predictor in the neural network (Section 3.3), but
333   instead to approximate biological activity through more general proxy variables such as temperature and
334   light availbility (see Table S2 in Supplementary Material). During June–August, as both the SPM and
335   Chl-a concentrations reach low values, the correlation weakens further, with August showing almost no
336   correlation at the shallow station. In November and December the correlation strengthens again as the
337   role of biological activity reduces and physical drivers become dominant again.
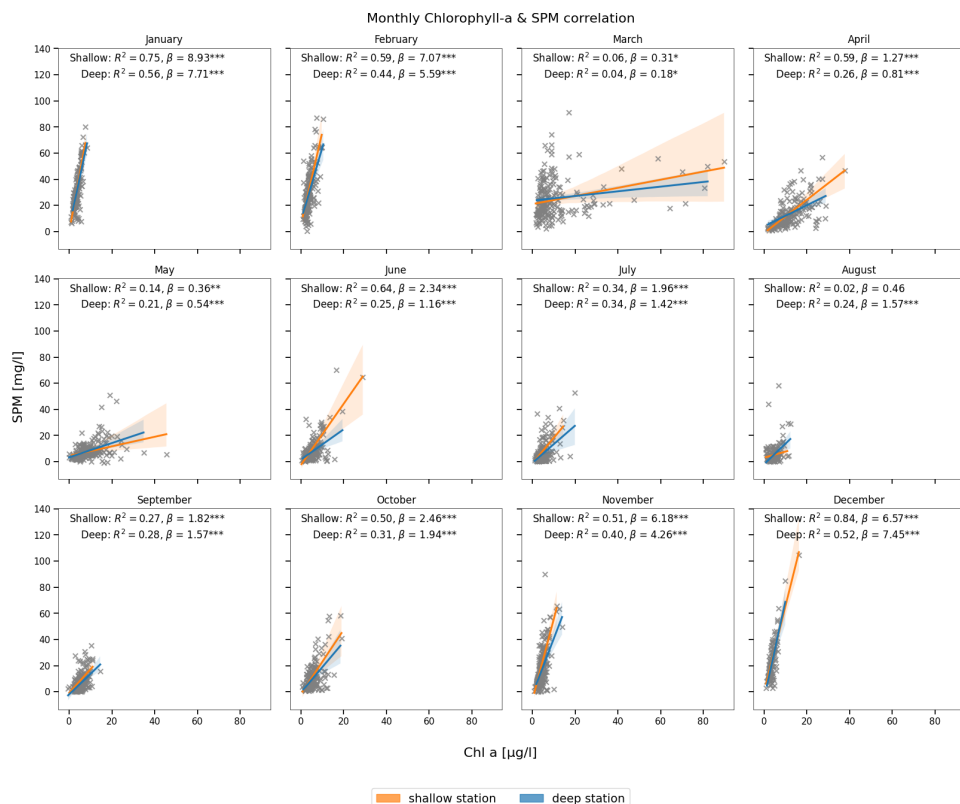
338
339 **Figure 4: Monthly correlation between Chl-a (x-axis) and SPM (y-axis) concentrations at the deep (blue) and shallow (orange)**
340 **stations. The coefficient of determination (R²), slope (β), and statistical significance (***p < 0.001, **p < 0.01, *p < 0.05) are**
341 **indicated in each panel.**

3.1.2 Role of wind forcing in seasonal SPM variations

The relationship between seasonal SPM concentrations and wind characteristics is illustrated in Fig. 5.
Wind speeds are highest in January, averaging around 8.5 ± 2.8 m/s, with peaks reaching 14.2 ± 1.7
m/s, and gradually decline through spring months, reaching a minimum with mean speeds around $6.5 \pm$
3.1 m/s and minima of 2.0 ± 0.7 m/s in July–August. From August onward, wind speeds begin to rise
again. This seasonal cycle aligns with the observed variability in SPM, with higher concentrations in
winter and lower values in summer. Dominant wind directions also vary throughout the year, with

349 westerly and northwesterly winds prevailing in most months, easterly winds in April, and more
350 southerly winds during October–November. Seasonal wind roses illustrating these patterns are shown in
351 the Supplementary Material (Fig. S1). However, no clear linear relationship emerges between dominant
352 wind direction and seasonal SPM concentrations. To account for potential non-linear interactions that
353 may still play a role, wind direction was included as an input feature in the NN model.
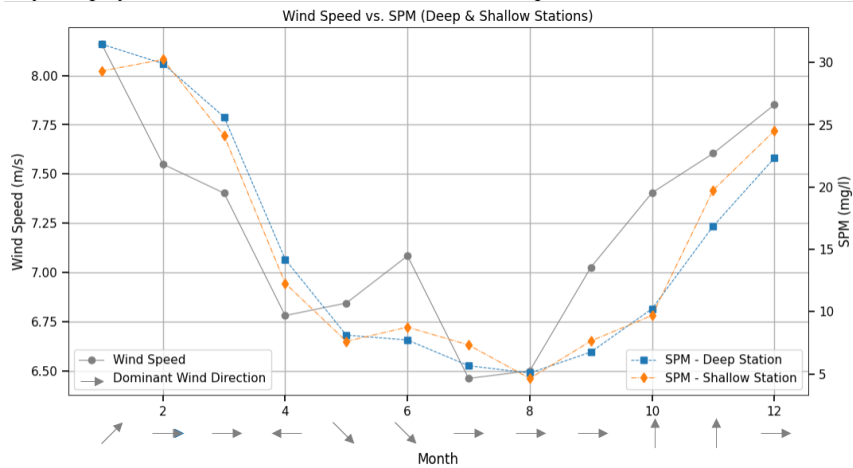
354
355 **Figure 5: Monthly averages of wind speed, SPM concentrations, and dominant wind direction (2000–2019). The figure illustrates**
356 **monthly mean wind speed (grey solid line, left axis) and SPM concentrations at the deep (blue squares) and shallow (orange**
357 **diamonds) stations (right axis). Grey arrows along the x-axis represent the dominant wind direction for each month, with arrow**
358 **orientation indicating the direction from which the wind originates, following standard meteorological convention.**

359 While correlations are further explored in Section 3.2, the seasonal alignment of wind intensity and
360 SPM concentrations suggests strong physical modulation.

361 **3.2 Resuspension and Time Scales of Inner Basin Transport**

362 Beyond seasonal variation, there are mechanisms responsible for the variability of SPM concentrations
363 on shorter temporal scales, from hours to days. This subsection examines how wind-induced
364 resuspension operates over different time frames and the role of tidal transport within the basin.

365 **3.2.1 Role of wind forcing in short time SPM variations**

366 To quantify the short-term response of SPM to wind forcing, we computed Pearson correlation
367 coefficients between SPM concentrations and wind speed averaged over different time intervals,
368 ranging from 1 hour to 240 hours. This approach, commonly referred to as "wind memory," allows us
369 to evaluate how the cumulative influence of past wind conditions affects SPM variability at different
370 depths and over varying time scales. Figure 6 illustrates how the strength of this relationship evolves as

373 wind speeds are averaged over progressively longer intervals, ranging from 1 hour to 240 hours. This
374 approach quantifies how SPM responds to the cumulative influence of past wind conditions over
375 varying time scales. The results show that correlation coefficients generally increase as wind memory
376 lengthens, reaching a peak around 12-18 hours at the shallow station and 120 hours at the deep station,
377 followed by a slight decline.
378 Monthly variations in the correlation patterns are provided in the Supplementary Material (Fig. S2),
379 showing that the correlation between wind speed and SPM is generally stronger in winter than in
380 summer, with more complex patterns during transitional months such as April and November.
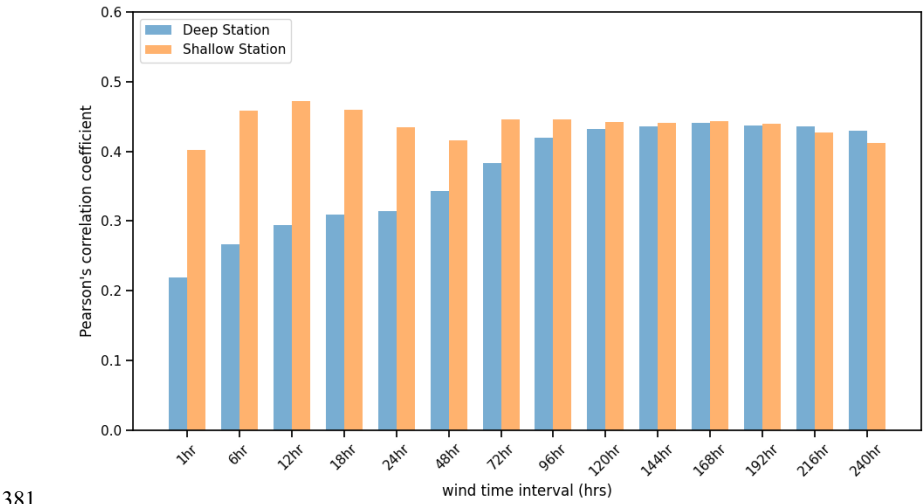
381
382 **Figure 6: Pearson correlation coefficients between SPM and wind speed averaged over different time intervals, ranging from 1**
383 **hour to 240 hours. The two stations (deep station as blue and shallow station as orange) are represented separately, showing how**
384 **wind memory influences SPM variability at different depths.**

385 The correlation between instantaneous wind speed and SPM concentrations is strongest during winter
386 and early spring (Fig. 7), particularly at the shallow station, where the most substantial value occurs in
387 January ($R^2 = 0.44$) and April ($R^2 = 0.50$). In contrast, the deep station shows much weaker correlations,
388 with R^2 values often near zero, reflecting a lagged effect on SPM concentrations.
389 During June–August, the relationship weakens significantly, with the lowest correlations observed in
390 August for both stations. The shallow station maintains minor correlation ($R^2 \approx 0.15$) into late summer
391 and early autumn.
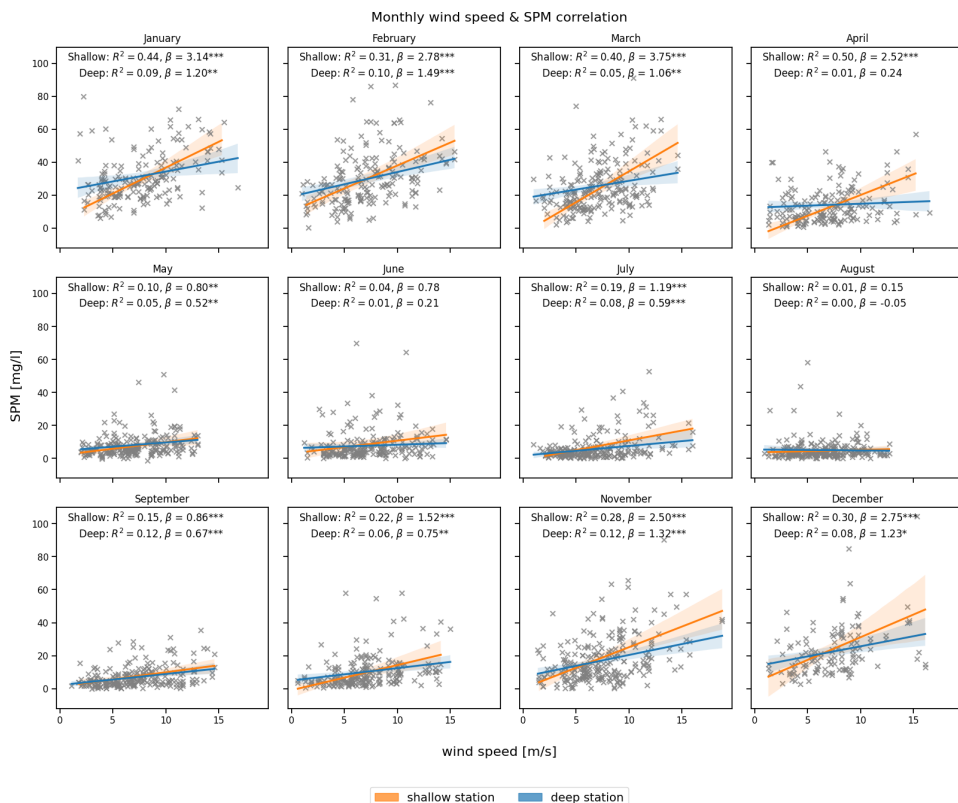
Figure 7: Monthly correlation between wind speed at the time of sampling (x-axis) and SPM concentration (y-axis) at the deep (blue) and shallow (orange) stations. The coefficient of determination (R^2), slope (β), and statistical significance (***p < 0.001, **p < 0.01, *p < 0.05) are indicated in each panel.

In contrast to the instantaneous impact of wind-speed, averaging wind speed over 120 hours (5 days) results in an improved correlation between wind and SPM at the deep station, as shown in Fig. 8, although the seasonal pattern remains similar. The stronger relationship is particularly evident in the winter and autumn months, especially at the deep station (e.g., $R^2 = 0.35$ in September, 0.24 in November and February). These findings indicate that the average wind-speed over several days have a stronger influence on SPM concentrations at the deep station than the wind at the time of sampling. The results highlight the role of wind forcing in modulating SPM concentration variability, particularly in shallow waters during winter and autumn. Naturally, the influence of wind is less pronounced in

408   deeper waters through direct resuspension mechanisms. However, it remains significant, with a time lag
409   possibly caused by the transport of resuspended material from shallower zones to the deep station.
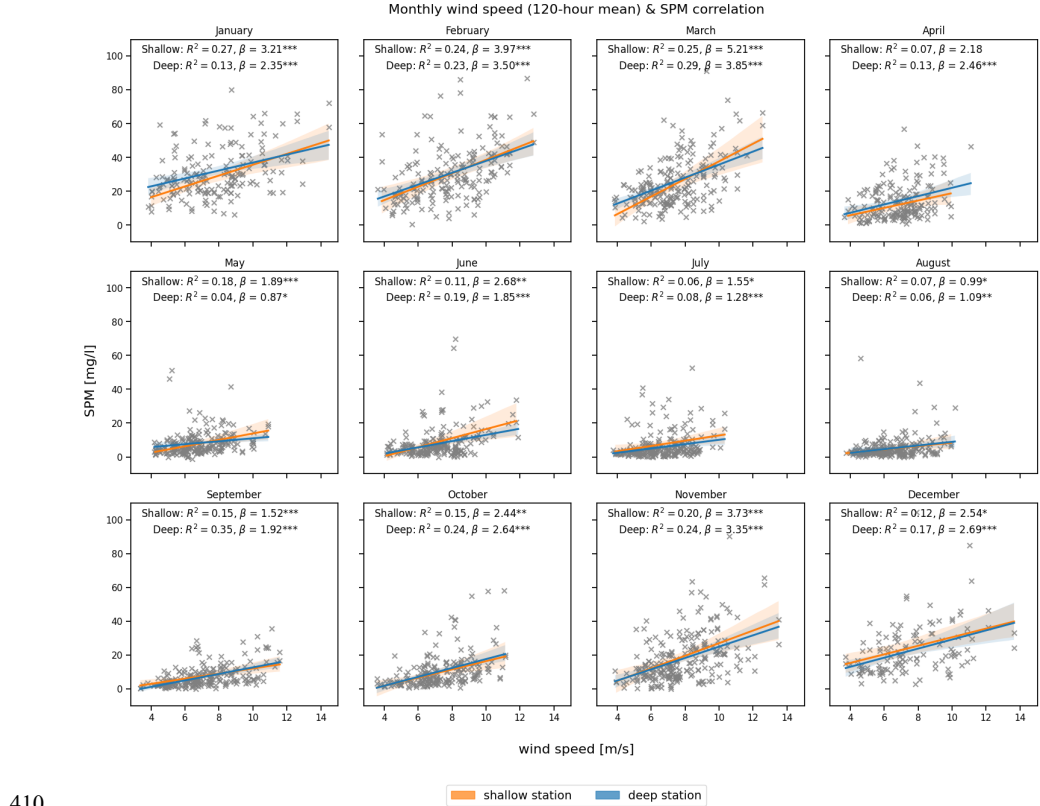
410
411   **Figure 8: Monthly correlation between wind speed averaged over a 120-hour (5-day) period (x-axis) and SPM concentration (y-**
412   **axis) at the deep (blue) and shallow (orange) stations. The coefficient of determination (R²), slope (β), and statistical significance**
413   **(***p < 0.001, **p < 0.01, *p < 0.05) are indicated in each panel.**

 3.2.2 Role of tidal forcing in short time SPM variations
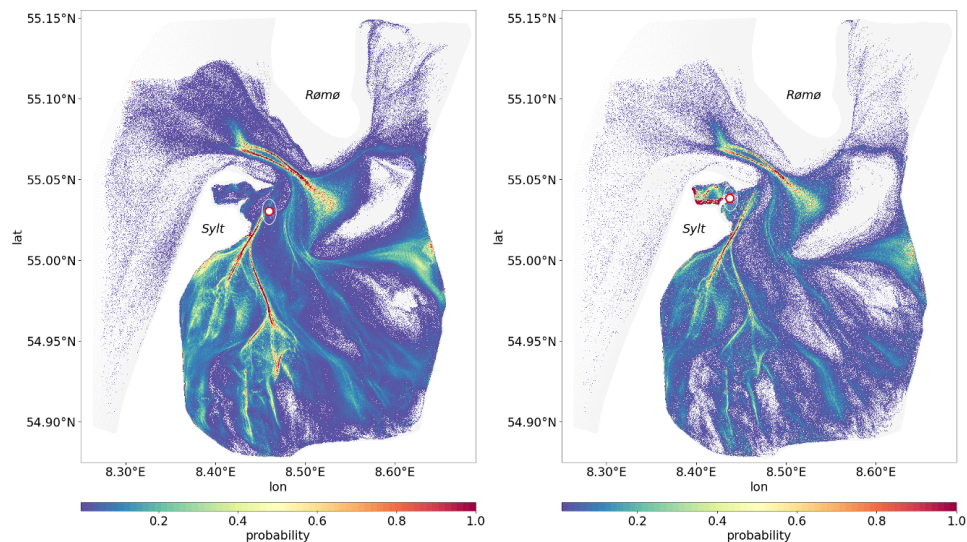
415
416 **Figure 9: Probability distribution of passive tracer pathways to illustrate how frequently different areas act as source regions or**
417 **transport corridors for passive tracers. Higher probability values (highlighted in yellow and red) indicate locations that more**
418 **frequently contribute to SPM reaching the deep station (left panel) or shallow station (right panel).**

419 Figure 9 shows the spatial probability distribution of passive tracer connectivity within the basin,
420 derived from Lagrangian simulations forced solely by tides. This setup isolates the dominant physical
421 driver of material transport in the Sylt-Rømø Bight, where tidal processes account for roughly 80% of
422 velocity variability (Fofonova et al., 2019). While regular wind forcing (excluding storm events and
423 uncommon multi-day episodes of strong winds from a single direction) enhances lateral dispersion, its
424 net contribution to basin-wide transport over several days is relatively minor (Konyssova et al., 2025).
425 Note, in this region, typical wind events last about 5–6 hours, defined as consecutive hours of wind
426 from the same direction within an eight-sector classification (Rubinetti et al., 2023). Residual currents
427 generated by non-linear tidal interactions establish consistent, directional transport pathways, which are
428 effectively captured by the simulated tracer trajectories.
429 The resulting network of tidally-induced transport pathways reveals apparent differences between the
430 two stations. The shallow station is predominantly supplied by tracers originating in the northern parts
431 of the bight, particularly Königshafen and its surroundings, reflecting localized and relatively rapid
432 connections. In contrast, the deep station is influenced by broader and more distributed transport
433 pathways, integrating material from a wider area of the basin.
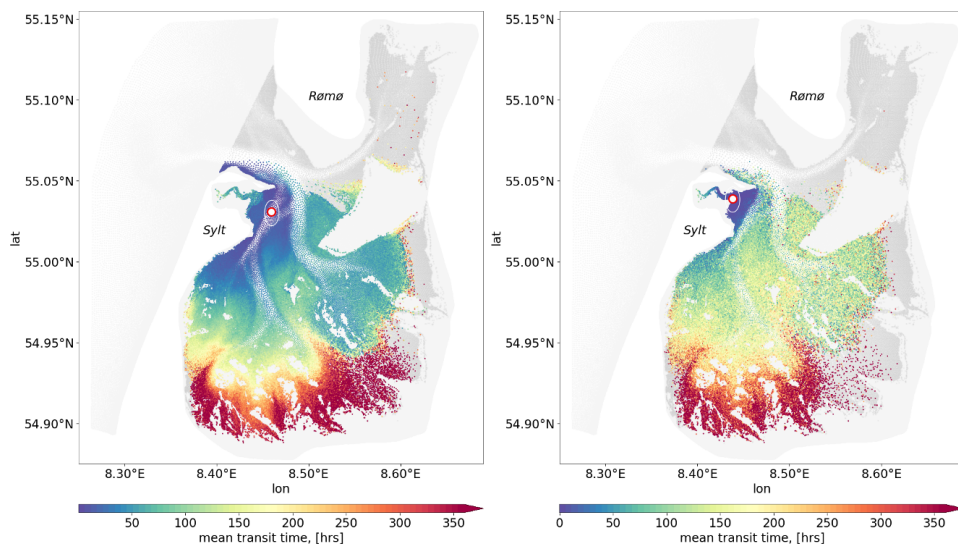
Figure 10: The mean transit time of passive tracers to reach the sampling station. The left panel corresponds to the deep station, while the right panel represents the shallow station. Grid elements that are consistently inundated with each flood phase, from which the passive tracers are released, are shown in grey. Elements that successfully reach one of the two sampling stations are colour-coded by their mean transit time (in hours), reflecting how long it takes for passive tracers to reach from a given location to each station.

For both stations, shorter transit times (depicted in blue and green, Fig. 10) are observed in areas closer to the stations, whereas regions further away, particularly in the inner tidal flats, exhibit longer transit times (yellow to red hues, Fig. 10). The transit time patterns reveal that SPM originating from intertidal areas and tidal channels follows particular pathways before reaching the deeper and shallower monitoring stations, with transport occurring on timescales of days to weeks. The difference between the two panels suggests that the deep and shallow stations receive material from primarily distinct but partially overlapping source regions.

Together, these figures illustrate the tidal connectivity of the two monitoring stations with their surrounding basin, highlighting likely source regions and typical transport pathways. To quantify the typical timescale for SPM transport, a probability-weighted transit time was computed, where individual transit times were weighted according to their interpolated probability values. This approach ensures that the estimated transit time reflects the most frequently occurring transport pathways rather than rare, low-probability trajectories. The resulting probability-weighted median transit time was 133.3 hours for the deep station, which aligns with the ~5-day wind-memory interval identified in Section 3.2.2, and 44.4 hours for the shallow station, highlighting the pronounced contrast in transport efficiency between the two locations and likely reflecting differences in sediment source regions. Although not explicitly resolved in the simulations, this difference may also relate to grain-size

457 composition, as the deeper channels typically contain coarser material, whereas the intertidal flats have
458 finer, more cohesive sediments (Bartholomä et al., 2009). At the shallow station, which is situated
459 within the Königshafen area, SPM concentrations respond to wind forcing almost immediately through
460 local resuspension. The longer transit time therefore does not indicate a delayed response, but rather
461 reflects the additional supply of tracers arriving from a wider surrounding area, which extends the
462 median transit time beyond the short wind-driven response captured in the memory analysis. In contrast,
463 the deep station integrates SPM from more complex, multi-step transport routes over longer timescales.
464 These transit times provide a key reference for interpreting observed SPM fluctuations at each station
465 and may help distinguish between short-term and cumulative drivers of SPM variability.

466 **3.3 Neural Network**

467 **3.3.1 Winter SPM prediction (Baseline Model)**
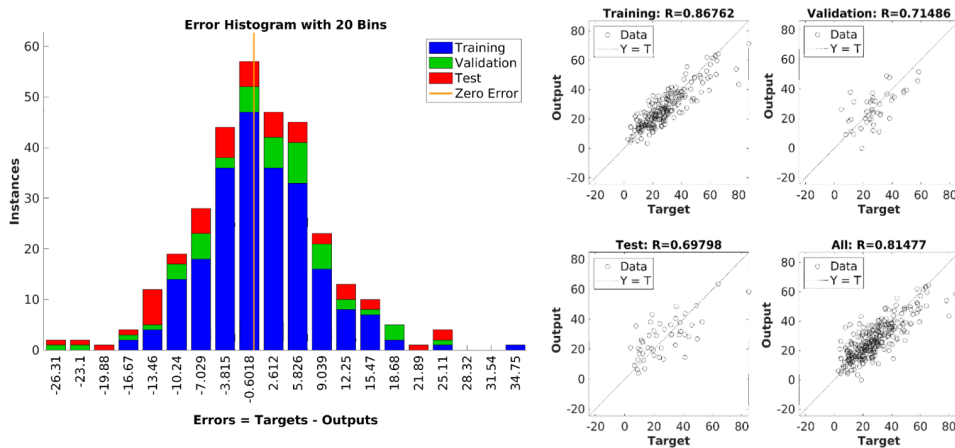
468
469 **Figure 11: Performance of the neural network (NN) trained on the winter dataset for the deep station. Left: Error histogram**
470 **showing the distribution of prediction errors (in mg/L) for training, validation, and test subsets. Right: Regression plots**
471 **comparing predicted vs. observed SPM values, with correlation coefficients (R) for each data subset. Due to the overall qualitative**
472 **similarity between the pictures for deep and shallow stations, only the deep station is presented here.**

473 To evaluate how well physical drivers alone can explain SPM concentration variability, we first trained
474 a baseline NN using only the winter dataset, when biological activity is minimal. This provides a
475 reference to assess the contribution of wind and tidal forcing under conditions with limited biological
476 influence.
477 The error for training, validation and testing has a normal distribution (Fig. 11, left). For the deep
478 station, the root mean square error (RMSE), a measure of average prediction error magnitude, is 9.4
479 mg/L for the testing set. Note that the observed mean and median SPM concentrations in winter are 27.6

481   and 25.9 mg/L respectively. As a result of the application of NN to the winter dataset, they are 27.2 and
482   25.5 mg/L respectively (Table 2). Regression analysis (Fig. 11, right) yields correlation coefficients
483   between observed and simulated SPMs equal to ~0.87, ~0.71, ~0.7 and ~0.81 for training, validation,
484   testing and all winter datasets, respectively.
485   The results show that, by using tidal and wind forcing along with a proxy for baroclinic conditions
486   (salinity), we can predict SPM concentrations during winter quite well without accounting for other
487   factors.
488   Notably, temperature, salinity, turbulent kinetic energy, and SPM concentrations themselves all
489   influence flocculation processes, even without considering biological activity. Temperature was
490   excluded from the feature set at this stage due to its strong seasonal cycle and its potential use as a
491   proxy for biological conditions. Specifically, in our current approach, we cannot separate the influence
492   of temperature on biological mechanisms from its physical effects (e.g. viscosity), which also impact
493   flocculation.

494   **3.3.2 Applying of NN trained on winter data to other seasons**

495   Next, we applied the NN trained under winter conditions to other seasons. This approach is justified by
496   the fact that the long-term dataset captures a representative range of wind conditions in both winter and
497   summer, including calm periods and strong wind events. Furthermore, salinity remains relatively stable
498   across seasons, supporting the applicability of the model. Using the trained winter model, we attempt to
499   predict SPM concentrations for spring, summer, and autumn. The goal of this step is to estimate the
500   influence of biological processes on SPM concentrations.
501   For both stations, the results of the NN application show significantly higher SPM concentrations
502   compared to observations (Table 2).

503   **Table 2. Mean, median values and correlation (R) of SPM concentrations, [mg/L], from observations VS predictions by NN**
504   **trained on winter dataset for the deep and shallow stations**

seasons		Deep Station		Shallow Station	
		observed	predicted	observed	predicted
winter	mean, [mg/L]	27.6	27.2	28.5	24.7
	median, [mg/L]	25.9	25.5	24.4	26.5
		R = 0.81		*R = 0.81*	
spring	mean, [mg/L]	16.5	24.8	15.6	20.6
	median, [mg/L]	13.3	24.3	11.3	18.0
		R = 0.29		*R = 0.5*	
summer	mean, [mg/L]	6.15	17.7	6.8	18.5
	median, [mg/L]	4.22	16.9	3.9	16.1
		R = 0.04		*R = 0.35*	

autumn	mean, [mg/L]	11.6	23.4	12.8	24.0
	median, [mg/L]	8.5	22.7	7.5	21.0
		R = 0.44		R = 0.54	
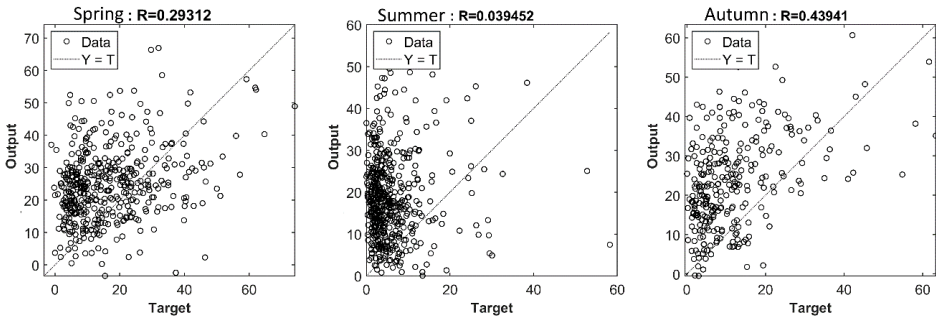
Figure 12: Regression analysis for NN trained on winter data and applied to spring, summer and autumn data vs observations. Results shown for the deep station; shallow station results are qualitatively similar and summarized in Table 2.

This discrepancy suggests that while calmer wind conditions alone can explain approximately 40% of the SPM reduction in summer compared to winter, they do not account for the full ~80% decrease observed in the data (see Table 2). The overestimation of SPM by the NN is clearly visible in the regression plots (Fig. 12), where most of the predicted values are positioned above the Y = T line, particularly during summer and autumn. This does not necessarily imply that biological activity is weaker in spring, but rather that its impact is less well captured by the abiotic-only model, as biological processes contribute more strongly to variability than in autumn. The higher correlation between simulated and observed SPM in autumn likely reflects physical conditions that are more similar to winter, when the model was trained, including generally stronger winds (Section 3.2.2). In spring, enhanced biological activity and aggregation introduce variability that the model cannot account for, reducing correlation. During summer, the regression coefficient dropping below 0.05 indicates that processes not represented in the abiotic model become dominant (Fig. 12). The subsequent analysis of all seasons presented in Section 3.3.3 points to biologically mediated mechanisms, such as flocculation and sediment stabilization, as the main contributors to this variability.

3.3.3 NN trained at the data from all seasons

Previously we showed that there are factors, in particular biological processes, which significantly influence the SPM dynamics. To confirm this, we trained NN on all the dataset (not limited to winter) using the same input features representing only abiotic conditions, which we used in 3.3.1. As expected, the overall RMSE increases to approximately 11 mg/L, due to the omission of important features that influence SPM dynamics during the warm season (Supplementary Fig. S5). When the model is trained on data from all seasons, and applied specifically to winter conditions, it

Deleted: biological processes become the primary driver of SPM concentration variability, as evidenced by the regression coefficient

Deleted: dropping below 0.05 (Fig. 12).

532 underestimates SPM concentrations. For the deep station, the predicted mean and median are 19.17
533 mg/L and 17.2 mg/L, respectively, compared to observed values of 27.6 mg/L and 25.9 mg/L. At the
534 shallow station, the model yields mean and median predictions of 20 mg/L and 17 mg/L, whereas the
535 corresponding observed values are 28.45 mg/L and 24.35 mg/L. The regression coefficients also reflect
536 this underperformance, with values of approximately $R \approx 0.66$ (deep) and 0.72 (shallow). The seasonal
537 regression analysis further highlights these biases (Supplementary Fig. S7, upper row). A complete
538 numerical breakdown of observed and predicted seasonal values is provided in Table S3.

3.3.4 Neural network trained on all-season data including biological proxy features

540 Including temperature and sunshine duration as proxies for biological activity improved overall model
541 skill, reducing the test RMSE to ~10 mg/L. The regression analysis shows the correlation coefficient
542 between observed and simulated SPM concentrations reached ~0.88, ~0.76, ~0.72 and ~0.84 for
543 training, validation, testing and all datasets respectively (Supplementary Fig. S6).
544 Seasonal regression plots also show marked improvements (Supplementary Fig. S7, lower row). For
545 winter, R increased from 0.66 to 0.73 at the deep station and from 0.72 to 0.82 at the shallow station.
546 The largest gains occurred in spring and summer, consistent with more substantial biological influence
547 during these seasons. Table S3 provides the detailed seasonal comparison of observed and predicted
548 means, medians, and correlations.

4 Discussion

550 This study set out to investigate the combined influence of wind forcing, tidal transport, and biological
551 processes on SPM concentration variability in the Sylt-Rømø Bight. Using 20-year period monitoring
552 data and applying statistical tools, neural network models, and Lagrangian simulations, we analyze the
553 relative roles of these processes across seasonal and short-term timescales.
554 The variability observed in SPM concentrations reflects the inherent complexity of the system, where
555 several physical and biological mechanisms interact across different spatial and temporal scales. Wind-
556 driven resuspension, tidal advection, and biologically mediated effects each contribute to the observed
557 dynamics, with their relative importance shifting seasonally. This complexity highlights that the
558 variability in SPM concentrations cannot be attributed to a single driver but rather to the combined
559 response of the system to multiple, overlapping processes.
560 In this chapter, we will further discuss topics that have not yet been fully addressed: the peculiarities of
561 the Chl-a and SPM concentration relationship, biological processes that directly or indirectly influence
562 SPM dynamics, further details on wind and tide control including SSH and SPM concentration
563 relationship, details of NN related findings and study limitations.

4.1 Biological Interaction

565 The strong positive correlation between Chl-a and SPM concentrations in winter suggests that under
566 low biological activity, such as limited phytoplankton growth, behaviour of both variables is driven
567 mainly by physical processes such as wind-driven resuspension. This is consistent with previous

569 observations in the Wadden Sea and German Bight (van Beusekom et al., 1999; van Beusekom and de
570 Jonge, 2002). Together with SPM, the strong winds resuspend microphytobenthos attached to sediment
571 particles (de Jonge and van Beuseukom, 1995), consistent with observations by Hommersom et al.
572 (2009), who found strong correlations between SPM and Chl-a in the Wadden Sea driven by
573 resuspension. Such patterns support the interpretation that, under winter conditions with low biological
574 production, a large fraction of Chl-a is contained within resuspended flocs, leading to the high
575 correlations observed in our study at both stations. In contrast, the correlation between Chl-a and SPM
576 concentrations begin to decline in spring, despite persistent wind forcing, and reaches a minimum in
577 summer. This seasonal decoupling suggests that biological aggregation processes become increasingly
578 dominant with the beginning of and following phytoplankton bloom, promoting the formation and
579 subsequent rapid settling of flocs (Schartau et al., 2019; Maerz et al., 2016; Lunau et al., 2006). For
580 example, the production of TEPs, secreted by phytoplankton and bacteria under certain physiological or
581 nutrient conditions, strongly enhance particle stickiness and promote the aggregation of both organic
582 and mineral particles (Passow, 2002). While our statistical analysis (however, not NN related efforts)
583 uses Chl-a as a proxy for biological activity, it is worth noting that TEP production responds to
584 additional drivers such as nutrient status and species composition, which can modulate flocculation
585 potential even at similar Chl-a levels. In addition to the biological feedback, the increase in water
586 temperature during summer also accelerates particle sinking rates by reducing water viscosity, further
587 promoting sediment deposition (Maerz and Wirtz, 2009). This supports the view that the Chl-a–SPM
588 relationship reflects an interplay of multiple biological and physical controls rather than a single, direct
589 pathway.
590 While both spring and autumn are characterized by peaks in Chl-a concentration, their influence on
591 SPM dynamics appears to differ. In spring, calmer conditions favor particle aggregation and settling,
592 often leading to reduced SPM levels. In autumn, however, the secondary bloom coincides with a
593 seasonal increase in wind speed (Fig. 5), resulting in elevated SPM concentrations despite high
594 biological activity. This suggests that enhanced organic matter availability in autumn may promote
595 flocculation, but stronger resuspension prevents effective settling. These seasonal contrasts highlight
596 that biological influence on SPM is strongly modulated by concurrent physical forcing.
597 In parallel, benthic microbial processes such as biofilm formation by microphytobenthos enhance
598 sediment stability and reduce its susceptibility to resuspension, thereby modulating the amount of SPM
599 remaining in the water column (Andersen, 2000; Stal, 2010). Beyond microbial stabilization, benthic
600 fauna also influences SPM dynamics through benthic-pelagic coupling. Filter-feeding benthos, such as
601 bivalves, consume suspended particulate organic carbon (POC), effectively removing material from the
602 water column and altering vertical fluxes of organic matter. In the Sylt-Rømø Bight, food web
603 modelling by Baird et al. (2004) estimated that benthic consumers remove approximately 56.7 mgC m^{-2}
604 d^{-1} of suspended POC – potentially a substantial fraction of total SPM, depending on the proportion of
605 organic material within it. Benthic consumption likely constitutes a significant sink for fine, organic-
606 rich particles, particularly in areas with dense benthic communities, as filter feeders remove SPM
607 primarily through ingestion and the production of faecal pellets, which promote deposition of organic-
608 rich material to seabed. Although the proportion of POC within SPM is known to depend on total SPM
609 concentration (Schartau et al., 2019), robust SPM-to-POC conversion factors remain uncertain due to
610 the unknown share of freshly formed organic matter. Although the effects of native species on bentho-

611 pelagic coupling have been relatively well studied in the region (Baird et al., 2007), the role of
612 introduced species remains less clear. For example, the introduction and spread of alien species such as
613 the American razor clam (*Ensis leei*) may further amplify benthic filtration effects. In the Dutch
614 Wadden Sea, they have shown to significantly alter trophic carbon flows, increasing carbon
615 consumption by secondary producers and redirecting energy flows away from higher trophic levels
616 (Jung et al., 2020). Although the abundance of *E. leei* in the Sylt-Rømø Bight has not yet been
617 quantified, its potential influence on observed SPM concentrations provides a basis for further
618 investigation as part of long-term ecological changes in the region.

4.2 Wind & Tide Control

620 The results suggest that the intensity of winds, rather than their dominant directions, exerts a stronger
621 influence on the seasonal cycle of SPM. The seasonal patterns of wind speed, with maximum values in
622 winter and minima in summer, aligns closely with the observed SPM concentrations, suggesting a
623 physically mediated control during high-energy periods. During summer, the weaker relationship
624 between wind speed and SPM concentrations points to the increasing importance of biological
625 contribution. These may include enhanced flocculation and settling of particles, increased filtration by
626 benthic organisms, reduced sediment availability due to biological stabilization, and overall calmer
627 wind conditions. Although tidal forcing itself does not vary seasonally, its influence on SPM
628 concentrations also likely changes throughout the year because the sediment properties and biological
629 activity that determine sediment availability and erodibility vary over time.
630 Notably, correlations between wind speed and SPM are stronger at the shallow station compared to the
631 deep station, as the shallow environments are more susceptible to wind-induced turbulence, including
632 wave action. It should be noted that, since the study addresses observations of SPM concentrations,
633 wind-induced resuspension is considered to include the effects of wave action.
634 In addition, the area around the shallow station is characterized by relatively small depths. Therefore, at
635 the shallow station, the short wind-memory intervals (12–18 hours) yield the strongest correlations.
636 Lagrangian simulations support this interpretation by illustrating that the shallow station, located within
637 the intertidal zone itself, receives SPM directly from resuspension at the site. While these simulations
638 do not represent full sediment dynamics, they effectively illustrate dominant source areas and transport
639 timescales. This relatively short response time aligns with earlier observations in tidal flat systems,
640 where wind effects on SPM are immediate in intertidal zones but take longer to become apparent in
641 deeper areas (de Jonge and van Beusekom, 1995).
642 In contrast, the situation at the deep station is more complex. In addition to the larger distance between
643 the observation point and the sea bottom, sediment characteristics in the channels are predominantly
644 sandy, which typically requires stronger wind energy to be resuspended as opposed to the mud and finer
645 material found in intertidal areas (Bartholomä et al., 2009). The delayed response seen in the wind
646 memory analysis (~120 hours) and the tidally modulated transport pathways from our Lagrangian
647 simulations (median transit time ~133 hours) likely reflects the combined influence of episodic wind-
648 driven resuspension in shallow areas and subsequent advective transport to the deeper station
649 (Friedrichs and Perry, 2001; de Jonge and van Beusekom, 1995). Similar multi-day lags in SPM
650 response have been observed in other estuarine systems where tidally dominated transport pathways act

652   on resuspended sediments originating from more energetic, nearshore zones (see also Winterwerp,
653   2001). Together, these results highlight a clear contrast between the two stations: rapid, localized
654   sediment response in the shallow embayment versus slower, more integrated transport processes at the
655   relatively deep channel.
656   The Lagrangian tracer simulations provide additional spatial context, revealing weak connectivity
657   between the north-eastern and southern sections of the Sylt-Rømø Bight under regular tidal conditions.
658   Passive tracers released in the north-eastern region rarely reach either of the sampling stations. This
659   indicates that the stations, while valuable for long-term monitoring, may not fully capture the spatial
660   variability of SPM dynamics across the entire basin, especially on shorter time scales.
661   Beyond local wind and tidal resuspension and transport within the Sylt-Rømø Bight, tidal phases also
662   influence SPM concentrations. Naturally, higher SPM concentrations are associated with lower water
663   levels under otherwise equal conditions, as the measurements are always taken at the surface (Fig. S3).
664   Due to the large role of non-linear processes in the area there is also an asymmetry between flood and
665   ebb in terms of duration as well as mean and maximum velocities.

666   **4.3 Neural Network findings**

667   The NN experiments provide a line of evidence supporting the seasonal shift in dominant SPM drivers
668   independent of the statistical analysis. When trained only on winter data, where biological activity is
669   minimal, the NN successfully captured winter SPM concentrations using solely physical drivers such as
670   wind conditions within different time intervals, salinity, and tidal elevation (through SSH and SSH
671   gradient). At both stations, this winter model performed well ($R \approx 0.81$), confirming that physical
672   processes alone can account for most of the observed variability during this season. This reinforces the
673   view that winter dynamics are dominated by abiotic drivers.
674   However, when the same winter-trained model was applied to other seasons, it consistently
675   overestimated SPM concentrations, especially in summer when biological activity is high and wind
676   speed is generally weaker. For example, at the deep station, the observed mean SPM concentration
677   decreased by ~78%, whereas the model reproduced only a ~36% reduction, meaning that less than half
678   of the observed seasonal decline could be explained by abiotic factors. Similarly, at the shallow station,
679   observed SPM declined by 80%, while the model captured only a ~42% reduction, accounting for just
680   over half of the change. These mismatches underscore the increasing importance of biological drivers
681   during the summer months. Interestingly, although both stations showed similar magnitudes of
682   overestimation, the shallow station retained higher predictive skill ($R \approx 0.35$) than the deep station ($R \approx$
683   0.04) in summer. This difference likely reflects the stronger and more immediate influence of wind
684   forcing at the shallow site, where even in summer, intermittent wind events can rapidly mobilize
685   sediments.
686   The addition of biologically relevant features such as temperature and sunshine duration into the full-
687   year NN model, in Section 3.3.4, significantly improved its performance, especially at the shallow
688   station. While we do not explicitly resolve individual biological pathways, these proxies likely capture
689   their cumulative effects as seen from the improved model fit indicating their aggregate influence is both
690   detectable and substantial. These processes may include phytoplankton-driven aggregation and
691   flocculation, microbial stabilization, and bentho-pelagic interactions such as benthic filtration. Our

692   interpretation remains exploratory rather than conclusive, as targeted biological data would be required
693   to quantify these mechanisms in detail.

694   **4.4 Study Limitations**

695   Although, in this study, we discuss the main driving mechanisms of SPM concentrations in the Sylt-
696   Rømø Bight, we also acknowledge that the system is far more complex and has more factors
697   influencing the fluctuations of SPM concentrations than we investigate here. Moreover, the SPM itself
698   is a parameter that is composed of various components and sizes in nature, and such a level of detail is
699   not readily available in the dataset. Incorporating measurements of sediment composition (organic
700   versus inorganic fractions) and their sizes would add more certainty into the roles of considered
701   mechanisms modifying SPM concentrations.
702   Our Lagrangian transport simulations use massless passive tracers, which do not account
703   for flocculation, deposition, or resuspension processes. Incorporating such processes would require a
704   different modeling framework and additional data that are not currently available, including detailed
705   habitat maps and reliable estimates of SPM fluxes from the open boundary. Nonetheless, despite these
706   simplifications, the model effectively captures key patterns of spatial connectivity pathways and
707   timescales driven by tidal dynamics.
708   Another limitation is that changes in the SPM input from the open boundary cannot be quantified. Net
709   coastward transport from the North Sea likely contributes to seasonal variability, for example, through
710   enhanced import or retention in spring and summer (Burchard et al., 2008; Postma, 1981), but we lack
711   data to resolve this numerically.
712   In addition, more precise SPM predictions would benefit from neural network architectures with
713   "memory", such as Long Short-Term Memory (LSTM) models, which can account for the delayed
714   effects of biotic and abiotic conditions over several months. A North Sea-wide approach would be
715   required to capture these long-term dynamics and boundary-driven influences. Within such a
716   framework, it would also be appropriate to include additional predictors such as nutrient concentrations
717   and benthic processes to represent better the complex interactions driving SPM variability.
718   While this study does not claim to offer a comprehensive representation of all the processes in play, we
719   believe that our work presents new insights to understand better the baseline mechanisms of SPM
720   concentration variability within the basin and across multiple timescales.

721   **5 Conclusions**

722   This study investigated the primary drivers of SPM variability in the Sylt-Rømø Bight, a semi enclosed
723   basin with well-mixed conditions and hydrodynamics dominantly shaped by tides. We combined long-
724   term monitoring data (SPM, Chl-a, wind conditions, and light availability) with SSH reconstructed from
725   a validated hydrodynamic model, and applied statistical analyses and neural network modelling. In
726   addition, Lagrangian transport simulations were used to assess tidal connectivity and transport
727   timescales. Together, these approaches revealed new insights on SPM concentration variability across
728   multiple timescales and relative influence of the main driving mechanisms.

729 Our findings confirm that wind speed is the primary driver of short-term SPM variability, particularly at
730 the shallow station, where SPM concentrations respond almost immediately to wind forcing. This rapid
731 response, especially during winter and autumn, highlights the importance of wind-driven resuspension
732 in shallow waters. In contrast, the deep station exhibits a more delayed response to wind forcing, with
733 peak correlations occurring at longer wind memory intervals (~5 days). This lag reflects the fact that, at
734 greater depths, direct resuspension due to immediate wind forcing plays a reduced role, while the
735 transport of material from neighboring shallower areas becomes increasingly important.
736 Tidal dynamics primarily regulate the advection processes within the basin, redistributing fine, easily
737 resuspendable material from shallow to the deeper areas. Lagrangian simulations illustrate that SPM at
738 the shallow station originates locally, predominantly from within or around the Königshafen
739 embayment. Meanwhile, at the deep station, SPM is likely supplied from the intertidal and shallow
740 areas by the tidally driven redistribution over a longer timescale (~133 hours), consistent with the
741 observed wind-memory lag (~120 hours). These results highlight the fundamental distinction
742 between localized, wind-driven resuspension and slower, broader-scale, tide-driven transport, both of
743 which shape SPM variability but at different spatial and temporal scales.
744 On seasonal timescales, however, biological processes exert an increasingly strong control. The onset of
745 the spring phytoplankton bloom coincides with a decline in SPM concentrations, likely due to the
746 enhanced production of TEPs and other extracellular polymers that promote biological aggregation and
747 flocculation, leading to enhanced particle settling. This strengthening of biological effects reduces the
748 efficiency of physical resuspension even under comparable wind conditions, which results in the
749 pronounced decline in SPM concentrations toward summer. The inverse seasonal patterns of Chl-a and
750 SPM support this interpretation, aligning with previous studies that describe the role of phytoplankton
751 in promoting flocculation and sedimentation in coastal systems. NN experiments suggest that calmer
752 wind conditions alone can explain approximately ~40% of the observed summer SPM reduction
753 compared to winter concentrations. Still, they do not account for up to ~80% decrease seen in the data.
754 This substantial reduction is likely influenced by a variety of biologically related mechanisms, ranging
755 from the microbial activity, production of EPS to zooplankton grazing. Further studies are needed to
756 quantify the relative contributions of these individual mechanisms.
757 Overall, this study provides a comprehensive and quantitative assessment of how wind, tides, and
758 biological activity interact to control SPM variability in a shallow, tidally dominated coastal system.

Conflict of Interest

760 The authors declare that they have no conflict of interest.

Author Contributions

762 GK performed the data analysis and wrote the initial draft of the manuscript. GK, VS, and AA carried
763 out the numerical simulations. JvB, GK, and VS conceptualized the study. SH, SR, IK, and KHW
764 contributed to the discussion of methods and interpretation of the results. All authors contributed to
765 manuscript review and editing.

Funding

This study has been funded by the German Federal Ministry of Education and Research (BMBF) in the frame of the joint research projects MGF-Nordsee (FKZ 03F0847A), CREATE (03F0910B) and Coastal Futures (FKZ 03F0911J) part of the research mission "Protection and Sustainable use of Marine Areas", within the German Marine Research Alliance (DAM).

Data Availability

The source code of the FESOM-C model is publicly available via Zenodo: https://doi.org/10.5281/zenodo.2085177 (Androsov et al., 2018). The Sylt Roads observational dataset is accessible through the PANGAEA data portal: https://doi.org/10.1594/PANGAEA.873549, https://doi.org/10.1594/PANGAEA.873547, https://doi.org/10.1594/PANGAEA.918018, https://doi.org/10.1594/PANGAEA.918032, https://doi.org/10.1594/PANGAEA.918027, https://doi.org/10.1594/PANGAEA.918023, https://doi.org/10.1594/PANGAEA.918033, https://doi.org/10.1594/PANGAEA.918028, https://doi.org/10.1594/PANGAEA.918024, https://doi.org/10.1594/PANGAEA.918034, https://doi.org/10.1594/PANGAEA.918029, https://doi.org/10.1594/PANGAEA.918025, https://doi.org/10.1594/PANGAEA.918035, https://doi.org/10.1594/PANGAEA.918030, https://doi.org/10.1594/PANGAEA.918026, https://doi.org/10.1594/PANGAEA.918036, and https://doi.org/10.1594/PANGAEA.918031. Meteorological data, including hourly wind characteristics (station 3032, List auf Sylt; dataset ID: *urn:x wmo:md:de.dwd.cdc::obsgermany-climate-hourly-wind*) and daily sunshine duration (*urn:wmo:md:de-dwd-cdc:obsgermany-climate-daily-kl*), are available from the Climate Data Center (CDC) of the Deutscher Wetterdienst (DWD): https://opendata.dwd.de/climate_environment/. The Lagrangian model output and Neural Network results are available from the corresponding author upon reasonable request.

Acknowledgements

We thank the teams involved in the Sylt Roads long-term ecological monitoring program for providing essential in-situ data. We also acknowledge the Deutscher Wetterdienst (DWD) Climate Data Center for access to freely available meteorological datasets. This study was conducted as part of the research mission "Protection and Sustainable Use of Marine Areas" of the German Marine Research Alliance (DAM) and was financially supported by the German Federal Ministry of Education and Research (BMBF).

References

Aarup, T.: Transparency of the North Sea and Baltic Sea - a Secchi depth data mining study, Oceanologia, 44, 323–337, 2002.

803 Andersen, T. J.: The role of fecal pellets in sediment settling at an intertidal mudflat, the Danish
804 Wadden Sea, in: Proceedings in Marine Science, vol. 3, edited by: McAnally, W. H. and Mehta, A. J.,
805 Elsevier, 387–401, https://doi.org/10.1016/S1568-2692(00)80133-3, 2000.

806 Androsov, A., Fofonova, V., Kuznetsov, I., Danilov, S., Rakowsky, N., Harig, S., Holger, B., and
807 Wiltshire, K.H.: FESOM-C, , https://doi.org/10.5281/ZENODO.2085177, 2018.

808 Androsov, A., Fofonova, V., Kuznetsov, I., Danilov, S., Rakowsky, N., Harig, S., Brix, H., and
809 Wiltshire, K. H.: FESOM-C v.2: coastal dynamics on hybrid unstructured meshes, Geosci. Model Dev.,
810 12, 1009–1028, https://doi.org/10.5194/gmd-12-1009-2019, 2019.

811 Baird, D., Asmus, H., and Asmus, R.: Energy flow of a boreal intertidal ecosystem, the Sylt-Rømø
812 Bight, Mar. Ecol. Prog. Ser., 279, 45–61, https://doi.org/10.3354/meps279045, 2004.

813 Baird, D., Asmus, H., and Asmus, R.: Trophic dynamics of eight intertidal communities of the Sylt-
814 Rømø Bight ecosystem, northern Wadden Sea, Mar. Ecol. Prog. Ser., 351, 25–41,
815 https://doi.org/10.3354/meps07137, 2007.

816 Bale, A., Morris, A., and Howland, R.: Seasonal sediment movement in the Tamar Estuary,
817 Oceanologica Acta, 8, 1–6, 1985.

818 Bartholomä, A., Kubicki, A., Badewien, T. H., and Flemming, B. W.: Suspended sediment transport in
819 the German Wadden Sea—seasonal variations and extreme events, Ocean Dynamics, 59, 213–225,
820 https://doi.org/10.1007/s10236-009-0193-6, 2009.

821 Becherer, J., Flöser, G., Umlauf, L., and Burchard, H.: Estuarine circulation versus tidal pumping:
822 Sediment transport in a well-mixed tidal inlet, JGR Oceans, 121, 6251–6270,
823 https://doi.org/10.1002/2016JC011640, 2016.

824 Bruns, I., Bartholomä, A., Menjua, F., and Kopf, A.: Physical impact of bottom trawling on seafloor
825 sediments in the German North Sea, Front. Earth Sci., 11, 1233163,
826 https://doi.org/10.3389/feart.2023.1233163, 2023.

827 Burchard, H., Flöser, G., Staneva, J. V., Badewien, T. H., and Riethmüller, R.: Impact of Density
828 Gradients on Net Sediment Transport into the Wadden Sea, Journal of Physical Oceanography, 38, 566–
829 587, https://doi.org/10.1175/2007JPO3796.1, 2008.

830 Cadée, G. C.: Increased phytoplankton primary production in the Marsdiep area (Western Dutch
831 Wadden Sea), Netherlands Journal of Sea Research, 20, 285–290, https://doi.org/10.1016/0077-
832 7579(86)90050-5, 1986.

833   Christiansen, C., Vølund, G., Lund-Hansen, L. C., and Bartholdy, J.: Wind influence on tidal flat
834   sediment dynamics: Field investigations in the Ho Bugt, Danish Wadden Sea, Marine Geology, 235,
835   75–86, https://doi.org/10.1016/j.margeo.2006.10.006, 2006.

836   Cloern, J. E.: Turbidity as a control on phytoplankton biomass and productivity in estuaries, Continental
837   Shelf Research, 7, 1367–1381, https://doi.org/10.1016/0278-4343(87)90042-2, 1987.

838   Colijn, F.: Light absorption in the waters of the Ems-Dollard estuary and its consequences for the
839   growth of phytoplankton and microphytobenthos, Netherlands Journal of Sea Research, 15, 196–216,
840   https://doi.org/10.1016/0077-7579(82)90004-7, 1982.

841   de Jonge, V. N.: Relations Between Annual Dredging Activities, Suspended Matter Concentrations, and
842   the Development of the Tidal Regime in the Ems Estuary, Can. J. Fish. Aquat. Sci., 40, s289–s300,
843   https://doi.org/10.1139/f83-290, 1983.

844   de Jonge, V. N. and van Beusekom, J. E. E.: Wind- and tide-induced resuspension of sediment and
845   microphytobenthos from tidal flats in the Ems estuary, Limnol. Oceanogr., 40, 776–778,
846   https://doi.org/10.4319/lo.1995.40.4.0776, 1995.

847   de Jonge, V. N. and de Jong, D. J.: 'Global Change' Impact of Inter-Annual Variation in Water
848   Discharge as a Driving Factor to Dredging and Spoil Disposal in the River Rhine System and of
849   Turbidity in the Wadden Sea, Estuarine, Coastal and Shelf Science, 55, 969–991,
850   https://doi.org/10.1006/ecss.2002.1039, 2002.

851   Depestele, J., Ivanović, A., Degrendele, K., Esmaeili, M., Polet, H., Roche, M., Summerbell, K., Teal,
852   L. R., Vanelslander, B., and O'Neill, F. G.: Measuring and assessing the physical impact of beam
853   trawling, ICES Journal of Marine Science, 73, i15–i26, https://doi.org/10.1093/icesjms/fsv056, 2016.

854   Dissanayake, D. M. P. K., Ranasinghe, R., and Roelvink, J. A.: The morphological response of large
855   tidal inlet/basin systems to relative sea level rise, Climatic Change, 113, 253–276,
856   https://doi.org/10.1007/s10584-012-0402-z, 2012.

857   Dolch, T. and Reise, K.: Long-term displacement of intertidal seagrass and mussel beds by expanding
858   large sandy bedforms in the northern Wadden Sea, Journal of Sea Research, 63, 93–101,
859   https://doi.org/10.1016/j.seares.2009.10.004, 2010.

860   Dronkers, J.: Tidal asymmetry and estuarine morphology, Netherlands Journal of Sea Research, 20,
861   117–131, https://doi.org/10.1016/0077-7579(86)90036-0, 1986.

862   Dyer, K. R.: Chapter 14 Sediment Transport Processes in Estuaries, in: Developments in
863   Sedimentology, vol. 53, Elsevier, 423–449, https://doi.org/10.1016/S0070-4571(05)80034-2, 1995.

864 Egbert, G. D. and Erofeeva, S. Y.: Efficient Inverse Modeling of Barotropic Ocean Tides, J. Atmos.
865 Oceanic Technol., 19, 183–204, https://doi.org/10.1175/1520-
866 0426(2002)019<0183:EIMOBO>2.0.CO;2, 2002.

867 Eisma, D.: Flocculation and de-flocculation of suspended matter in estuaries, Netherlands Journal of
868 Sea Research, 20, 183–199, https://doi.org/10.1016/0077-7579(86)90041-4, 1986.

869 Engel, A. and Schartau, M.: Influence of transparent exopolymer particles (TEP) on sinking velocity of
870 Nitzschia closterium aggregates, Mar. Ecol. Prog. Ser., 182, 69–76,
871 https://doi.org/10.3354/meps182069, 1999.

872 Fettweis, M., Monbaliu, J., Baeye, M., Nechad, B., and van Den Eynde, D.: Weather and climate
873 induced spatial variability of surface suspended particulate matter concentration in the North Sea and
874 the English Channel, Methods in Oceanography, 3–4, 25–39, https://doi.org/10.1016/j.mio.2012.11.001,
875 2012.

876 Flöser, G., Burchard, H., and Riethmüller, R.: Observational evidence for estuarine circulation in the
877 German Wadden Sea, Continental Shelf Research, 31, 1633–1639,
878 https://doi.org/10.1016/j.csr.2011.03.014, 2011.

879 Fofonova, V., Androsov, A., Sander, L., Kuznetsov, I., Amorim, F., Hass, H. C., and Wiltshire, K. H.:
880 Non-linear aspects of the tidal dynamics in the Sylt-Rømø Bight, south-eastern North Sea, Ocean Sci.,
881 15, 1761–1782, https://doi.org/10.5194/os-15-1761-2019, 2019.

882 Friedrichs, C. T. and Aubrey, D. G.: Non-linear tidal distortion in shallow well-mixed estuaries: a
883 synthesis, Estuarine, Coastal and Shelf Science, 27, 521–545, https://doi.org/10.1016/0272-
884 7714(88)90082-0, 1988.

885 Friedrichs, C. and Perry, J.: Tidal salt marsh morphodynamics: a synthesis, Journal of Coastal Research,
886 27, 7–37, 2001.

887 Graf, G. and Rosenberg, R.: Bioresuspension and biodeposition: a review, Journal of Marine Systems,
888 11, 269–278, https://doi.org/10.1016/S0924-7963(96)00126-1, 1997.

889 Hagen, R., Winter, C., and Kösters, F.: Changes in tidal asymmetry in the German Wadden Sea, Ocean
890 Dynamics, 72, 325–340, https://doi.org/10.1007/s10236-022-01509-9, 2022.

891 Hommersom, A., Peters, S., Wernand, M. R., and de Boer, J.: Spatial and temporal variability in bio-
892 optical properties of the Wadden Sea, Estuarine, Coastal and Shelf Science, 83, 360–370,
893 https://doi.org/10.1016/j.ecss.2009.03.042, 2009.

894 Jansen, H., van Den Bogaart, L., Hommersom, A., and Capelle, J.: Spatio-temporal analysis of sediment
895 plumes formed by mussel fisheries and aquaculture in the western Wadden Sea, Aquacult. Environ.
896 Interact., 15, 145–159, https://doi.org/10.3354/aei00458, 2023.

897 Jeffrey, S. W. and Humphrey, G. F.: New spectrophotometric equations for determining chlorophylls a,
898 b, c1 and c2 in higher plants, algae and natural phytoplankton, Biochemie und Physiologie der Pflanzen,
899 167, 191–194, https://doi.org/10.1016/S0015-3796(17)30778-3, 1975.

900 Jung, A., van Der Veer, H., Philippart, C., Waser, A., Ens, B., de Jonge, V., and Schückel, U.: Impacts
901 of macrozoobenthic invasions on a temperate coastal food web, Mar. Ecol. Prog. Ser., 653, 19–39,
902 https://doi.org/10.3354/meps13499, 2020.

903 Konyssova, G., Sidorenko, V., Androsov, A., Sander, L., Danilov, S., Rubinetti, S., Burchard, H.,
904 Winter, C., Wiltshire, K.H.: Changes in tidal dynamics in response to sea level rise in the Sylt-Rømø
905 Bight (Wadden Sea), Ocean Dynamics, 75, 43, https://doi.org/10.1007/s10236-025-01688-1, 2025.

906 Kuznetsov, I., Androsov, A., Fofonova, V., Danilov, S., Rakowsky, N., Harig, S., and Wiltshire, K. H.:
907 Evaluation and Application of Newly Designed Finite Volume Coastal Model FESOM-C, Effect of
908 Variable Resolution in the Southeastern North Sea, Water, 12, 1412,
909 https://doi.org/10.3390/w12051412, 2020.

910 Kuznetsov, I., Rabe, B., Androsov, A., Fang, Y.-C., Hoppmann, M., Quintanilla-Zurita, A., Harig, S.,
911 Tippenhauer, S., Schulz, K., Mohrholz, V., Fer, I., Fofonova, V., and Janout, M.: Dynamical
912 reconstruction of the upper-ocean state in the central Arctic during the winter period of the MOSAiC
913 expedition, Ocean Sci., 20, 759–777, https://doi.org/10.5194/os-20-759-2024, 2024.

914 Lettmann, K. A., Wolff, J.-O., and Badewien, T. H.: Modeling the impact of wind and waves on
915 suspended particulate matter fluxes in the East Frisian Wadden Sea (southern North Sea), Ocean
916 Dynamics, 59, 239–262, https://doi.org/10.1007/s10236-009-0194-5, 2009.

917 Loebl, M., Dolch, T., and van Beusekom, J. E. E.: Annual dynamics of pelagic primary production and
918 respiration in a shallow coastal basin, Journal of Sea Research, 58, 269–282,
919 https://doi.org/10.1016/j.seares.2007.06.003, 2007.

920 Lunau, M., Lemke, A., Dellwig, O., and Simon, M.: Physical and biogeochemical controls of
921 microaggregate dynamics in a tidally affected coastal ecosystem, Limnol. Oceanogr., 51, 847–859,
922 https://doi.org/10.4319/lo.2006.51.2.0847, 2006.

923 Maerz, J., Hofmeister, R., van Der Lee, E. M., Gräwe, U., Riethmüller, R., and Wirtz, K. W.: Maximum
924 sinking velocities of suspended particulate matter in a coastal transition zone, Biogeosciences, 13,
925 4863–4876, https://doi.org/10.5194/bg-13-4863-2016, 2016.

Maerz, J. and Wirtz, K.: Resolving physically and biologically driven suspended particulate matter dynamics in a tidal basin with a distribution-based model, Estuarine, Coastal and Shelf Science, 84, 128–138, https://doi.org/10.1016/j.ecss.2009.05.015, 2009.

Neder, C., Fofonova, V., Androsov, A., Kuznetsov, I., Abele, D., Falk, U., Schloss, I. R., Sahade, R., and Jerosch, K.: Modelling suspended particulate matter dynamics at an Antarctic fjord impacted by glacier melt, Journal of Marine Systems, 231, 103734, https://doi.org/10.1016/j.jmarsys.2022.103734, 2022.

Passow, U.: Transparent exopolymer particles (TEP) in aquatic environments, Progress in Oceanography, 55, 287–333, https://doi.org/10.1016/S0079-6611(02)00138-6, 2002.

Pawlowicz, R., Beardsley, B., and Lentz, S.: Classical tidal harmonic analysis including error estimates in MATLAB using T_TIDE, Computers & Geosciences, 28, 929–937, https://doi.org/10.1016/S0098-3004(02)00013-4, 2002.

Postma, H.: Sediment transport and sedimentation in the estuarine environment, American Association of Advanced Sciences, 83, 158–179, 1967.

Postma, H.: Exchange of materials between the North Sea and the Wadden Sea, Marine Geology, 40, 199–213, https://doi.org/10.1016/0025-3227(81)90050-5, 1981.

Purkiani, K., Becherer, J., Flöser, G., Gräwe, U., Mohrholz, V., Schuttelaars, H. M., and Burchard, H.: Numerical analysis of stratification and destratification processes in a tidally energetic inlet with an ebb tidal delta, J. Geophys. Res. Oceans, 120, 225–243, https://doi.org/10.1002/2014JC010325, 2015.

Rick, J. J., Scharfe, M., Romanova, T., van Beusekom, J. E. E., Asmus, R., Asmus, H., Mielck, F., Kamp, A., Sieger, R., and Wiltshire, K. H.: An evaluation of long-term physical and hydrochemical measurements at the Sylt Roads Marine Observatory (1973–2019), Wadden Sea, North Sea, Earth Syst. Sci. Data, 15, 1037–1057, https://doi.org/10.5194/essd-15-1037-2023, 2023.

Rubinetti, S., Fofonova, V., Arnone, E., and Wiltshire, K. H.: A Complete 60-Year Catalog of Wind Events in the German Bight (North Sea) Derived From ERA5 Reanalysis Data, Earth and Space Science, 10, e2023EA003020, https://doi.org/10.1029/2023EA003020, 2023.

Schartau, M., Riethmüller, R., Flöser, G., van Beusekom, J. E. E., Krasemann, H., Hofmeister, R., and Wirtz, K.: On the separation between inorganic and organic fractions of suspended matter in a marine coastal environment, Progress in Oceanography, 171, 231–250, https://doi.org/10.1016/j.pocean.2018.12.011, 2019.

Sidorenko, V., Rubinetti, S., Akimova, A., Pogoda, B., Androsov, A., Beng, K. C., Sell, A. F., Pineda-Metz, S. E. A., Wegner, K. M., Brand, S. C., Shama, L. N. S., Wollschläger, J., Klemm, K., Rahdarian, A., Winter, C., Badewien, T., Kuznetsov, I., Herrling, G., Laakmann, S., and Wiltshire, K. H.:

959 Connectivity and larval drift across marine protected areas in the German bight, North Sea: Necessity of
960 stepping stones, Journal of Sea Research, 204, 102563, https://doi.org/10.1016/j.seares.2025.102563,
961 2025.

962 Skogen, M., Ji, R., Akimova, A., Daewel, U., Hansen, C., Hjøllo, S., van Leeuwen, S., Maar, M.,
963 Macias, D., Mousing, E., Almroth-Rosell, E., Sailley, S., Spence, M., Troost, T., and van de Wolfshaar,
964 K.: Disclosing the truth: Are models better than observations?, Mar. Ecol. Prog. Ser., 680, 7–13,
965 https://doi.org/10.3354/meps13574, 2021.

966 Sprong, P. A. A., Fofonova, V., Wiltshire, K. H., Neuhaus, S., Ludwichowski, K. U., Käse, L.,
967 Androsov, A., and Metfies, K.: Spatial dynamics of eukaryotic microbial communities in the German
968 Bight, Journal of Sea Research, 163, 101914, https://doi.org/10.1016/j.seares.2020.101914, 2020.

969 Stal, L. J.: Microphytobenthos as a biogeomorphological force in intertidal sediment stabilization,
970 Ecological Engineering, 36, 236–245, https://doi.org/10.1016/j.ecoleng.2008.12.032, 2010.

971 Toullec, J., Vincent, D., Frohn, L., Miner, P., Le Goff, M., Devesa, J., and Moriceau, B.: Copepod
972 Grazing Influences Diatom Aggregation and Particle Dynamics, Front. Mar. Sci., 6, 751,
973 https://doi.org/10.3389/fmars.2019.00751, 2019.

974 Turner, J.: Zooplankton fecal pellets, marine snow and sinking phytoplankton blooms, Aquat. Microb.
975 Ecol., 27, 57–102, https://doi.org/10.3354/ame027057, 2002.

976 van Beusekom, J. E. E. and de Jonge, V. N.: Long-term changes in Wadden Sea nutrient cycles:
977 importance of organic matter import from the North Sea, in: Nutrients and Eutrophication in Estuaries
978 and Coastal Waters, edited by: Orive, E., Elliott, M., and de Jonge, V. N., Springer Netherlands,
979 Dordrecht, 185–194, https://doi.org/10.1007/978-94-017-2464-7_15, 2002.

980 van Beusekom, J. E. E., Brockmann, U. H., Hesse, K.-J., Hickel, W., Poremba, K., and Tillmann, U.:
981 The importance of sediments in the transformation and turnover of nutrients and organic matter in the
982 Wadden Sea and German Bight, Deutsche Hydrographische Zeitschrift, 51, 245–266,
983 https://doi.org/10.1007/BF02764176, 1999.

984 van Maren, D. S., van Kessel, T., Cronin, K., and Sittoni, L.: The impact of channel deepening and
985 dredging on estuarine sediment concentration, Continental Shelf Research, 95, 1–14,
986 https://doi.org/10.1016/j.csr.2014.12.010, 2015.

987 Verney, R., Lafite, R., and Brun-Cottan, J.-C.: Flocculation Potential of Estuarine Particles: The
988 Importance of Environmental Factors and of the Spatial and Seasonal Variability of Suspended
989 Particulate Matter, Estuaries and Coasts, 32, 678–693, https://doi.org/10.1007/s12237-009-9160-1,
990 2009.

991 Winterwerp, J. C.: Stratification effects by cohesive and noncohesive sediment, J. Geophys. Res., 106,
992 22559–22574, https://doi.org/10.1029/2000JC000435, 2001.

993 Wotton, R.: The Essential Role of Exopolymers (Eps) in Aquatic Systems, in: Oceanography and
994 Marine Biology, vol. 20042243, edited by: Gibson, R., Atkinson, R., and Gordon, J., CRC Press, 57–94,
995 https://doi.org/10.1201/9780203507810.ch3, 2004.